

THERMAL NON-EQUILIBRIUM EFFECTS ON THE FLOWFIELD STRUCTURE OF HYPERSONIC FORWARD-FACING STEP FLOW

Paulo H. M. Leite, phmineiro@lcp.inpe.br
Wilson F. N. Santos, wilson@lcp.inpe.br

National Institute for Space Research, Combustion and Propulsion Laboratory, Cachoeira Paulista-SP, 12630-000 BRAZIL

Abstract. *This work describes a computational investigation on low-density hypersonic flow over forward-facing steps. The impact of the step frontal-face height on the thermal non-equilibrium is examined by employing the Direct Simulation Monte Carlo (DSMC) method. Results for the non-equilibrium between rotational temperature, vibrational temperature, “parallel” temperature, “normal” temperature, and translational temperature are presented and discussed at length. “Parallel” temperature and “normal” temperature are kinetic temperatures associated with x and y coordinate directions in the flowfield. Results showed that the flowfield is in thermal non-equilibrium in the boundary layer and inside the shock wave. In contrast, thermal equilibrium was verified at the vicinity of the step base due to the flow compression in this region. It was also found that entropy generation regions are related to the thermal non-equilibrium regions in the flowfield.*

Keywords: *DSMC, Hypersonic Flow, Rarefield Flow, Non-Equilibrium Effects, Reentry, Forward-Facing Step.*

1. INTRODUCTION

Reentry hypersonic vehicles are thermally protected during reentry by a system made by tiles that are bounded to the aluminium structure. In order to account for the thermal expansion, surface discontinuities like cavities, gaps or steps are necessary between the individual tiles. Such surface discontinuities may affect locally the flowfield structure and may cause higher than expected heating on the vehicle surface during atmospheric reentry. In order to operate safely, these heating loads have to be predicted correctly. As a result, the evaluation of heating and pressure loads during reentry has always been one of the key issue in the design of reentry hypersonic vehicles.

For the particular case of forward-facing steps, many experimental and theoretical studies have been conducted in order to understand the physical aspects of a hypersonic flow past to this type of discontinuity, characterized by a sudden change on the surface slope. For the purpose of this introduction, it will be sufficient to describe only a few of these studies.

Nestler et al. (1969) conducted an experimental investigation on steps and cavities in a hypersonic turbulent flow. For the flow conditions investigated, they found that the pressure distributions in the cavity presented a typical behavior of closed cavity flow in the sense that the flow expands into the cavity, reattaches to the floor, and separates as it approaches the downstream corner.

Pullin and Harvey (1977) numerically analyzed a two-dimensional rarefied hypersonic flow around a forward-facing step by considering N_2 as the working fluid and freestream Mach number of 22. The analysis showed that in the vicinity of the step base, the flow has a rapid deceleration and compression accompanied by a sudden transition to a near continuum Navier-Stokes-type state nearly in equilibrium at the body temperature. The computational results presented good agreement with experimental data.

Grotowsky and Ballmann (2000) investigated laminar hypersonic flow over forward- and backward-facing steps by employing Navier-Stokes equations. The hypersonic flow over the steps were simulated by considering freestream Mach number of 8, Reynolds number of the order of 10^8 and an altitude of 30 km. According to them, the computational results presented a good agreement with the experimental data available in the literature. They also pointed out that the quantitative comparison exhibited major differences for the wall heat flux, probably due to the difficulty in how to measure accurately.

Leite and Santos (2009a) have studied forward-facing steps situated in a rarefied hypersonic flow by employing the DSMC method. The work was motivated by the interest in investigating the frontal-face height effects on the flowfield structure. The primary emphasis was to examine the sensitivity of the velocity, density, pressure and temperature due to step-height variations of such forward-facing steps. The analysis showed that the hypersonic flow past a forward-facing step was characterized by a strong compression ahead of the frontal face. It was found that the recirculation region ahead of the steps is a function of the frontal-face height. The analysis also showed that flow upstream disturbances depend on the frontal-face height of the steps. In addition, results showed that the separation point and the pre-separation region rely on the frontal-face height.

Leite and Santos (2009b) have extended the previous analysis (Leite and Santos, 2009a) by investigating the impact of the frontal-face height on the aerodynamic surface quantities. The primary goal was to assess the sensitivity of the heat transfer, pressure and skin friction coefficients to variations on the frontal-face height of the step. The analysis showed

that hypersonic flow past a forward-facing step is characterized by a strong compression ahead of the frontal face, which influences the aerodynamics surface properties upstream the frontal face. Locally high heating rates were observed on the surface upstream the step. It was found that the heating rate increased by increasing the frontal-face height of the steps.

The present investigation was undertaken in an attempt to expand further the previous analysis (Leite and Santos, 2009a) by investigating the impact of the step frontal-face height on the thermal non-equilibrium. In this scenario, the focus of this study is to assess the sensitivity of kinetic translational temperature T_T , rotational temperature T_R , vibrational temperature T_V and the kinetic temperatures associated with x and y coordinate directions in the flowfield, i.e., T_X and T_Y , to variations on the step frontal-face height. In addition, the investigation focuses on the physical aspects of hypersonic flow past to steps related to the severe aerothermodynamic environment associated to a reentry vehicle in the transition flow regime. These conditions are characterized by a thick laminar boundary layer approaching the step, i.e., the boundary layer thickness is larger than the step frontal-face height. In doing so, the Direct Simulation Monte Carlo (DSMC) method will be employed to calculate the hypersonic two-dimensional flow over the steps.

2. GEOMETRY DEFINITION

In the present account, the geometric parameters related to the forward-facing step are those presented in the previous studies, i.e., Leite and Santos (2009a,b). In this fashion, it was assumed that the step frontal-face height h is much smaller than the nose radius R of a reentry capsule, i.e., $h/R \ll 1$. Therefore, discontinuities on the surface of a reentry vehicles are considered herein as a hypersonic flow over a flat plate with a forward-facing step positioned far from the stagnation point. Figure 1(a) illustrates a schematic view of the model employed.

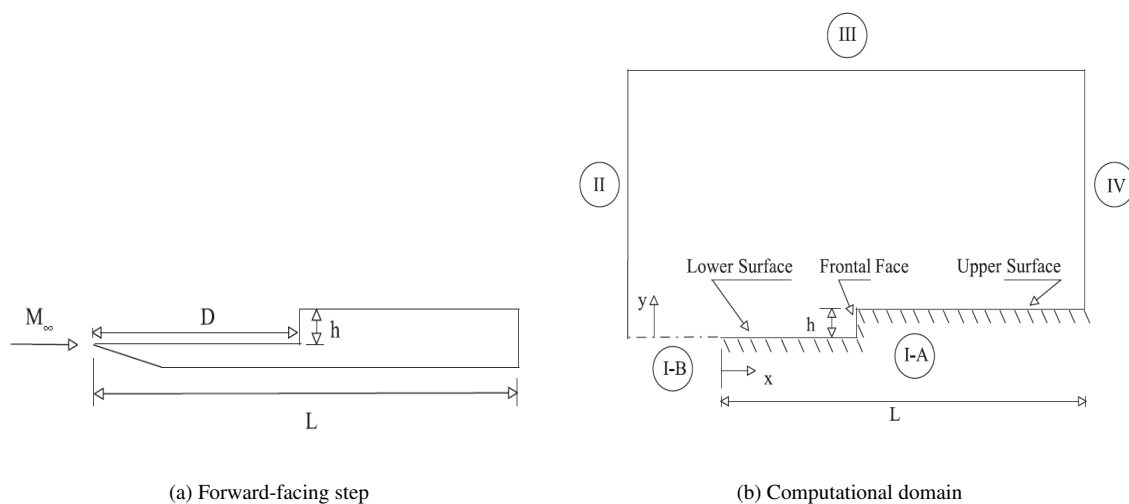


Figure 1. Drawing illustrating (a) the forward-facing step and (b) the computational domain.

According to Fig. 1(a), M_∞ represents the freestream Mach number, h the frontal-face height, L the total length of the forward-facing step, and D the location of the step. It was considered that the forward-facing step is infinitely long but only the length L is examined. It was assumed a frontal-face height h of 0, 3, 6, and 9 mm, which correspond to h/λ_∞ of 0, 3.23, 6.46 and 9.69, D/λ_∞ of 50 and L/λ_∞ of 100, where λ_∞ is the freestream mean free path. The especial case of $h/\lambda_\infty = 0$ corresponds to the flat-plate case free of surface discontinuities. Without a step, the flat-plate case works as a benchmark for the cases with steps.

2.1 COMPUTATIONAL METHOD AND PROCEDURE

The Direct Simulation Monte Carlo (DSMC) method, pioneered by (Bird, 1994), is a particle simulation method that aims to calculate practical gas flows through computations of motions and collisions of modeled molecules. DSMC has become one of the standard and reliable successful numerical techniques for rarefied gas flow simulations, and it has been applied to many fields. These include the traditional field of rarefied atmospheric gas dynamics, the emerging field of micro-fluidics and very-low pressure fields, such as space propulsion and vacuum systems.

The DSMC method is used for modeling complex flows in the transition flow regime and simulating real gas flows with various physical processes, by means of a huge number of simulated particles, where each simulated particle represents a fixed number of real gas particles. The transition flow regime is the category of flow that falls between the continuum flow regime, where the Navier-Stokes equations are valid, and the free-molecular flow regime, which is the limit of infinite

Knudsen number.

The DSMC method employs distribution functions to generate representative particles and to perform particle collisions. Sampling from a prescribed distribution is one of major tasks for the DSMC method. The commonly used sampling techniques is the acceptance-rejection method. The particle evolution is divided into two independent phases during the simulation: the movement phase and the collision phase. In the movement phase, all particles are moved over distances appropriate to a short time interval, time step, and some of them interact with the domain boundaries in this time interval. Particles that strike the solid wall would reflect according to the appropriate gas-surface interaction model; specular, diffuse or a combination of these. In the collision phase, intermolecular collisions are performed according to the theory of probability without time being consumed. In this way, the intermolecular collisions are uncoupled to the translational molecular motion over the time step used to advance the simulation. Time is advanced in discrete steps such that each step is small in comparison with the mean collision time (Hadjiconstantinou, 2000; Garcia and Wagner, 2000). In general, the total simulation time is identified with the physical time of the real gas flow. The simulation is always calculated as unsteady flow, however, a steady-flow solution is obtained as the large time state of the simulation.

In the present account, the molecular collision kinetics are modeled by using the variable hard sphere (VHS) molecular model (Bird, 1981), and the no time counter (NTC) collision sampling technique (Bird, 1989). Energy exchange between kinetic and internal modes is controlled by the Borgnakke-Larsen statistical model (Borgnakke and Larsen, 1975). Simulations are performed using a non-reacting gas model, consisting of 76.3% of N_2 and 23.7% of O_2 , while considering energy exchange between translational, rotational and vibrational modes. For a given collision, the probability is defined by the inverse of the number of relaxation, which corresponds to the number of collisions needed, on average, for a molecule undergoes relaxation. The probability of an inelastic collision determines the rate at which energy is transferred between the translational and internal modes after an inelastic collision. Relaxation collision numbers of 5 and 50 were used for the calculations of rotation and vibration, respectively.

2.2 COMPUTATIONAL DOMAIN AND GRID

For the numerical treatment of the problem, the flowfield around the forward-facing step is divided into an arbitrary number of regions, which are subdivided into computational cells. The cells are further subdivided into subcells, two subcells/cell in each coordinate direction. The cell provides a convenient reference for the sampling of the macroscopic gas properties, while the collision partners are selected from the same subcell for the establishment of the collision rate. The computational domain used for the calculation is made large enough so that body disturbances do not reach the upstream and side boundaries, where freestream conditions are specified. A schematic view of the computational domain is depicted in Fig. 1(b).

According to this figure, side I-A is defined by the body surface. Diffuse reflection with complete thermal accommodation is the condition applied to this side. In a diffuse reflection, the molecules are reflected equally in all directions, and the final velocity of the molecules is randomly assigned according to a half-range Maxwellian distribution determined by the wall temperature. Side I-B is a plane of symmetry, where all flow gradients normal to this plane are zero. At the molecular level, this plane is equivalent to a specular reflecting boundary. Sides II and III are the freestream side through which simulated molecules enter and exit. Finally, the flow at the downstream outflow boundary, side IV, is predominantly supersonic and vacuum condition is specified (Bird, 1994). At this boundary, simulated molecules can only exit.

Numerical accuracy in DSMC method depends on the grid resolution, on number of particles per computational cell as well as on the time step. In the DSMC code, the linear dimensions of the cells should be small in comparison with the scale length of the macroscopic flow gradients normal to the streamwise directions, which means that the cell dimensions should be of the order of or smaller than the local mean free path (Alexander et al, 1998; Alexander et al, 2000). The number of simulated particles has to be large enough to make statistical correlations between particles insignificant.

These effects were investigated in order to determine the number of cells and the number of particles required to achieve grid independence solutions. Grid independence was tested by running the calculations with half and double the number of cells in the coordinate directions compared to a standard grid. The effect of altering the cell size in the x -direction was investigated with grids of 100 (coarse), 200 (standard) and 400 (fine) cells, and 55 cells in the y -direction for the $h = 3$ mm case. In analogous fashion, an examination was made in the y -direction with grids of 28 (coarse), 55 (standard) and 110 (fine) cells, and 200 cells in the x -direction for the same case. From the total number of cells in the x -direction, 190 cells were located along side I-A and 10 cells distributed along side I-B. In addition, each grid was made up of a non-uniform cell spacing in both directions. The effect (not shown) of changing the cell size in both directions on the heat transfer, pressure and the skin friction coefficients was rather insensitive to the range of the cell spacing considered, indicating that the standard grid, 200 X 55 cells, for the $h = 3$ mm case, is essentially grid independent.

In the following, a similar examination was made for the number of molecules. The standard grid for the $h = 3$ mm case, 200 X 55 cells, corresponds to, on average, a total of 635,700 molecules. Two new cases using the same grid were investigated. These two new cases corresponded to 278,000 and 820,300 molecules in the entire computational domain. As the three cases presented approximately the same results (not shown) for the heat transfer, pressure and skin friction coefficients, hence the standard grid with a total of 635,700 molecules was considered enough for the calculations. A

discussion of these effects on the aerodynamic surface quantities for the other forward-facing steps presented herein is described in detail by Leite (2009).

3. FREESTREAM AND FLOW CONDITIONS

Freestream conditions employed in the present calculations are those given by Leite and Santos (2009a,b), and the gas properties follow those given by Bird (1994). For completeness, Tables 1 and 2 tabulate the freestream conditions and the gas properties, respectively. Referring to Tab. 1, U_∞ , T_∞ , p_∞ , ρ_∞ , μ_∞ , n_∞ and λ_∞ stand respectively for velocity, temperature, pressure, density, viscosity, number density and the molecular mean free path. Based on Tab. 2, X , m , d and ω account respectively for mass, molecular diameter and viscosity index.

Table 1. Freestream flow conditions

U_∞ (m/s)	T_∞ (K)	p_∞ (N/m ²)	ρ_∞ (kg/m ³)	μ_∞ (Ns/m ²)	n_∞ (m ⁻³)	λ_∞ (m)
7456	219.69	5.582	8.753×10^{-5}	1.455×10^{-5}	1.8192×10^{21}	9.285×10^{-4}

The freestream velocity U_∞ , assumed to be constant at 7456 m/s, corresponds to a freestream Mach number M_∞ of 25. The wall temperature T_W is assumed constant at 880 K. This temperature is chosen to be representative of the surface temperature near the stagnation point of a reentry capsule and is assumed to be uniform over the forward-facing-step surface. It is important to mention that the surface temperature is low compared to the stagnation temperature T_O of the air, i.e., $T_W/T_O = 0.013$. This assumption seems reasonable since practical surface material will probably be destroyed if surface temperature is allowed to approach the stagnation temperature.

By assuming the frontal-face height h as the characteristic length, the Knudsen number Kn_h corresponds to 0.3095, 0.1548 and 0.1032 for height h of 3, 6 and 9 mm, respectively. Finally, the Reynolds number Re_h , also based on the frontal-face height h and on conditions in the undisturbed stream, is around 136, 272, and 409 for height h of 3, 6 and 9 mm, respectively.

4. COMPUTATIONAL RESULTS AND DISCUSSION

It is usually accepted without questions that each law of thermodynamics is associated to the definition of a new system property. For instance, the internal energy is related to the first law, and entropy to the second law. In this fashion, the zeroth law defines the thermodynamic property called “temperature”.

Thermodynamic temperature is defined classically in terms of a reversible engine operating between two reservoirs by the following relation (Bejan, 1988),

$$\frac{T_1}{T_2} = \frac{Q_1}{Q_2} \quad (1)$$

where T is the temperature and Q is the amount of heat transferred.

Heat may be transferred either by conduction or radiation process. The conduction process is controlled by the translational energy of the molecules. On the other hand, radiation occurs by means of rotational, vibrational or electronic transitions, and is thus related to the corresponding energy distributions. According to the arguments of statistical mechanics, the energy of a gas is described by distribution functions for the various modes of energy storage. In order to characterize a distribution function by a single parameter, the temperature, each degree of freedom of the gas must be internally equilibrated. Nevertheless, the statistical description does not require equilibrium between modes of energy storage (Mates and Weatherston, 1965). In this way, one may speak of a translational temperature, a rotational temperature, a vibrational temperature, and so forth.

For a diatomic or polyatomic gas in complete thermodynamic equilibrium, the translational temperature is equal to the temperature related to the internal modes, i.e., rotational, vibrational or electronic temperatures, and it is identified as thermodynamic temperature. When the equilibrium is disturbed, relaxation processes arise in the system that attempt to return it to the state of the total statistical equilibrium. In diatomic or polyatomic gas, these are processes which results in the establishment of equilibrium with respect to individual degrees of molecular freedom such as translational, rotational,

vibrational or electronic. Conversely, in a thermodynamic non-equilibrium gas, an overall temperature is defined as the weighted mean of the translational and internal temperatures (Bird, 1994) as being,

$$T_{OV} = \frac{3T_T + \zeta_R T_R + \zeta_V T_V}{3 + \zeta_R + \zeta_V} \quad (2)$$

where ζ is the degree of freedom and subscript T , R and V stand for translation, rotation and vibration, respectively.

In the DSMC, translational, rotational, and vibrational temperatures are obtained to each cell in the computational domain by the following equations,

$$T_T = \frac{1}{3k} \sum_{j=1}^N \frac{(mc'^2)_j}{N} \quad (3)$$

$$T_R = \frac{2 \bar{\varepsilon}_R}{k \zeta_R} \quad (4)$$

$$T_V = \frac{\Theta_V}{\ln(1 + k\Theta_V/\bar{\varepsilon}_V)} \quad (5)$$

where k is the Boltzmann constant, c' is the thermal velocity of the molecules, Θ_V is the characteristic temperature of vibration, and $\bar{\varepsilon}_R$ and $\bar{\varepsilon}_V$ are, respectively, rotation and vibration average energies in each cell.

It is firmly established that a spacecraft entering into the atmosphere at hypersonic speed experiences two important features: (1) the strong shock wave that forms around the vehicle converts part of the kinetic energy of the freestream air molecules into thermal energy, the shock compression leads to strong molecular collisions. This thermal energy is partitioned into increasing the translational kinetic energy of the air molecules, and into exciting other molecular energy states such as rotation and vibration; (2) the low density of the atmosphere results in small molecular collision rates and, therefore, the thermal process may take place in local non-equilibrium conditions.

Having a clear qualitative picture of the physical features involved in a reentry hypersonic flow, the analysis now focuses on the temperature field on the forward-facing step, which represents one type of discontinuity on the surface of reentry vehicles. In doing so, temperature profiles for three sections along the lower surface of the steps are displayed in Fig. 2. In this set of plots, X represents the distance x normalized by the freestream mean free path λ_∞ , and Y the distance y above the lower surface also normalized by λ_∞ , temperature ratio stands for the translational temperature T_T , rotational temperature T_R , vibrational temperature T_V or overall temperature T_{OV} normalized by the freestream temperature T_∞ . Also, filled and empty symbols correspond to temperature distributions for height h of 3 and 9 mm, respectively.

It is apparent from this set of plots that thermodynamic non-equilibrium occurs throughout the shock layer, as shown by the lack of equilibrium of the translational and internal kinetic temperatures. Thermal non-equilibrium occurs when the temperatures associated with translational, rotational, and vibrational modes of a polyatomic gas are different.

Referring to Fig. 2, it should be recognized that, in the undisturbed freestream far from the lower surface, $Y \rightarrow \infty$, the translational and internal kinetic temperatures (rotational and vibrational) have the same value and are equal to the thermodynamic temperature. Approaching the lower surface, for instance, $Y \approx 2$ for section $X = 30$, the translational kinetic temperature rises to well above the rotational and vibrational temperatures, and reaches a maximum value that is a function of the section X . Since a large number of collisions is needed to excite molecules vibrationally from the ground state to the upper state, the vibrational temperature is seen to increase much more slowly than rotational temperature. The translational kinetic temperature rise results from the essentially bimodal velocity distribution: the molecular sample consisting of mostly undisturbed freestream molecules with the molecules that have been affected by the shock and reflected from the step surface. In this fashion, the translational kinetic temperature rise is a consequence of the large velocity separation between these two classes of molecules. The bimodal velocity distribution was pointed out by Liepmann et al. (1964).

Still further toward the lower surface, $Y \approx 0$, the translational and kinetic temperatures decrease, and reach values on the wall that are above the wall temperature $T_W (\approx 4T_\infty)$, resulting in a temperature jump as defined in continuum formulation. Nevertheless, at the vicinity of the step frontal-face, section $X = 48$, the difference between translational temperature and internal temperatures drastically decreases, and temperatures approach the wall temperature, indicating that the thermodynamic equilibrium is roughly achieved in this region. The reason for that comes from the fact that density dramatically increases at the vicinity of the step frontal face. As a result, the molecular collision rate also increases. As pointed out by Leite (2009), for the $h = 9$ mm case, the density ratio, ρ/ρ_∞ , increases from 1.8 to 52, as the section X changes from 30 to 48. Also, very close to the base of the steps, $X \approx 50$, density ρ is around 70 times the freestream density ρ_∞ .

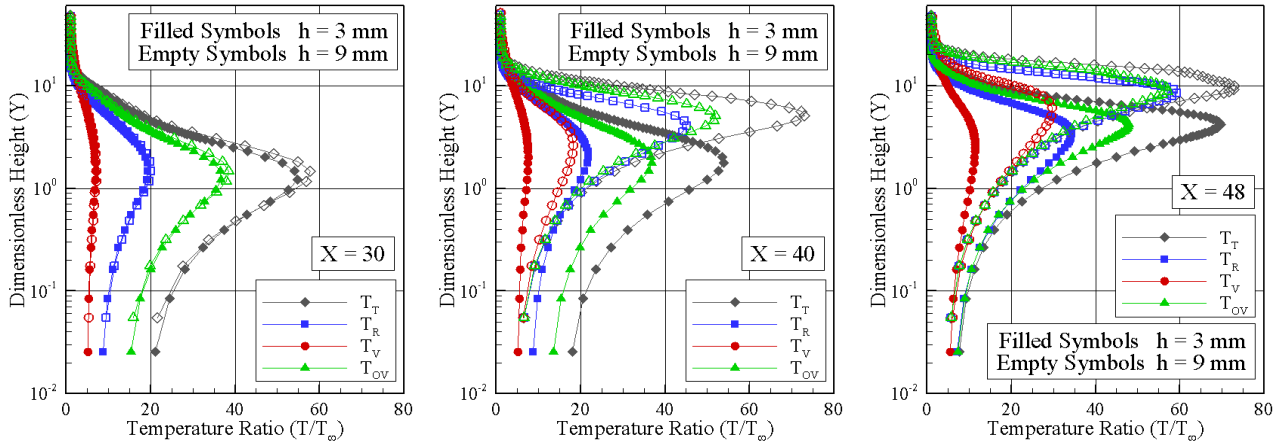


Figure 2. Distribution of kinetic temperature ratio (T/T_∞) profile along the lower surface of the forward-facing step as a function of the height h .

Still referring to Fig. 2, it is recognized that the downstream evolution of the flow along the lower surface displays a smearing tendency of the shock wave, formed at the leading edge of the lower surface, due to the displacement of the maximum value for the translational temperature.

In order to bring out the essential features of the thermal non-equilibrium at the vicinity of the forward-facing steps, the following temperature parameters are defined to highlight the impact of the step frontal height on the thermal non-equilibrium.

$$\eta_R = 1 - \frac{T_R}{T_T} \quad (6)$$

$$\eta_V = 1 - \frac{T_V}{T_T} \quad (7)$$

$$\eta_X = 1 - \frac{T_X}{T_T} \quad (8)$$

$$\eta_Y = 1 - \frac{T_Y}{T_T} \quad (9)$$

where the subscript X and Y stand, respectively, for translational temperature associated with x and y coordinate directions, i.e., “parallel” and “normal” temperatures.

Before looking at the problem in more detail, a brief consideration of the parameters η_X and η_Y is in order. The average kinetic energy associated with the thermal or translational motion of a molecule is $mc^2/2$, and the specific energy associated with this motion is $e_{tr} = \overline{c^2}/2$. In this way, the translational kinetic temperature is defined by the following expression,

$$\frac{3}{2}kT_{tr} = \frac{1}{2}m\overline{c^2} \quad (10)$$

Nevertheless, separate translational kinetic temperatures may be defined for each component associated with the coordinate directions as follows,

$$k\left(\frac{1}{2}T_{tr,x} + \frac{1}{2}T_{tr,y} + \frac{1}{2}T_{tr,z}\right) = \frac{1}{2}m(\overline{u^2} + \overline{v^2} + \overline{w^2}) \quad (11)$$

Therefore, the departure of these component temperatures from T_{tr} provides a measure of the degree of translational non-equilibrium. In the present account, T_{tr} , $T_{tr,x}$, and $T_{tr,y}$ are defined by T_T , T_X , and T_Y , respectively.

The distribution of non-equilibrium between rotational and translational temperatures, η_R , are demonstrated in Fig. 3 for three sections along the lower surface of the steps. For comparison purpose, this group of plots presents the parameter

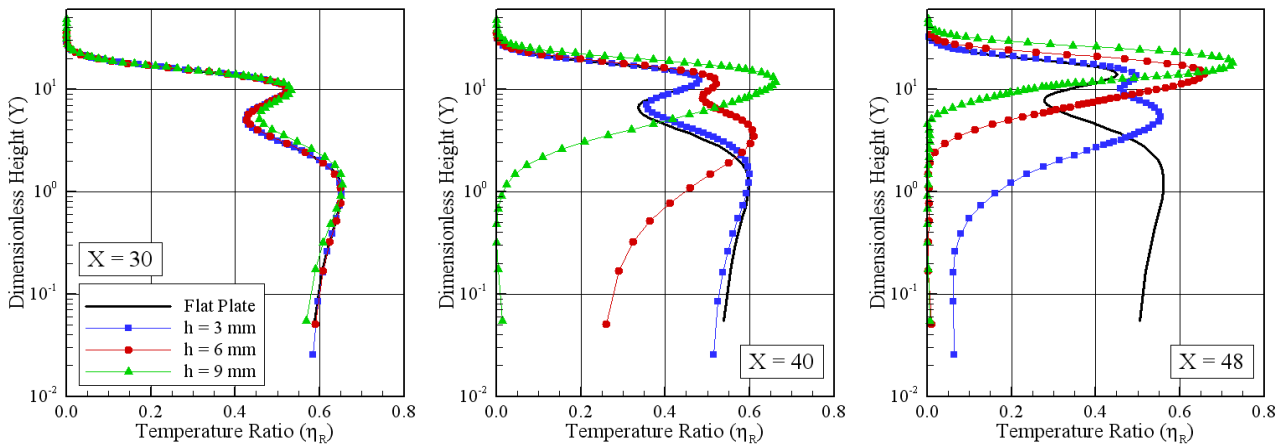


Figure 3. Distribution of η_R profiles for three sections along the step lower surface as a function of the height h .

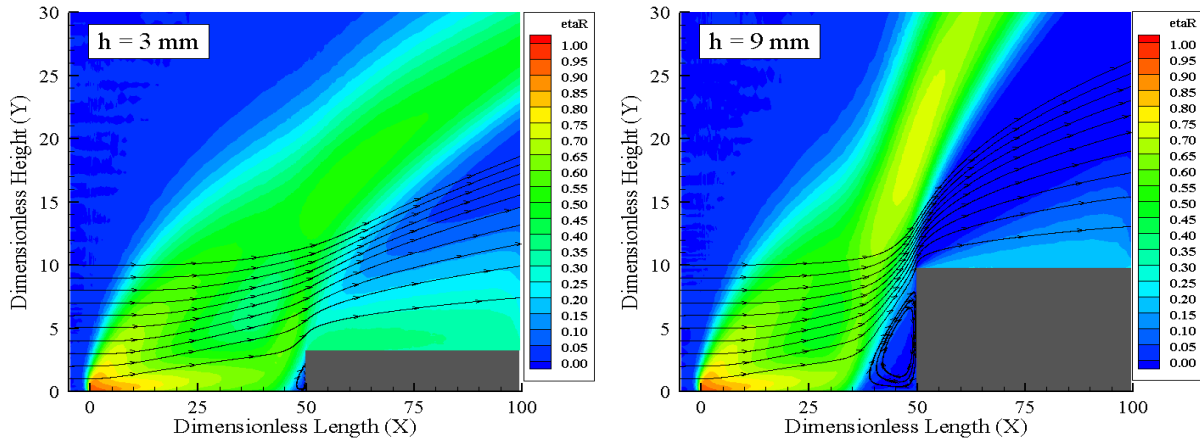


Figure 4. Non-equilibrium between rotational and translational temperatures, η_R , for a hypersonic flow over forward-facing steps with height h of 3 mm (left) and 9 mm (right).

η_R for the flat-plate case, i.e., a flat plate without a step. According to these plots, at section $X = 30$, it is seen that η_R profiles for the steps follow the same behavior as that presented by the flat-plate case. It is also seen that, at the vicinity of the lower surface, $Y \approx 0$, the parameter η_R is larger than zero, therefore, a thermal non-equilibrium region. In contrast, as $Y \rightarrow \infty$, $\eta_R \rightarrow 0$, indicating that rotational and translational temperatures are in thermal equilibrium. Nevertheless, as the flow approaches the step frontal face, it is noticed that rotational and translational temperatures reach the equilibrium conditions, since $\eta_R \rightarrow 0$ at the vicinity of the lower surface. As mentioned earlier, the reason for that comes from the fact that density dramatically increases at the base of the frontal face of the steps. Consequently, the local mean free path decreases, and the molecular collision rate increases. It should be remarked that, in the case of a diatomic gas with a finite rotational relaxation time, the rotational temperature must lag behind the translational temperature (Bird, 1994). For this particular study, the rotational relaxation collision number was set to five, as mentioned earlier.

In order to emphasize the distribution of thermal non-equilibrium associated with rotational temperature, Fig. 4 displays the contour map for η_R at the vicinity of the forward-facing steps defined by height h of 3 and 9 mm. The distribution for h of 6 mm is intermediate to the cases shown, and it will not be presented. According to these plots, the normalized temperature non-equilibrium parameter η_R becomes smaller far away from the step and the shock wave.

The distribution of non-equilibrium between translational and vibrational temperatures, η_V , are displayed in Fig. 5 for the same three sections along the lower surface of the steps. Based on this set of plots, it is noticed that η_V presents a similar behavior as that demonstrated by η_R in the sense that, at section $X = 30$, the profiles follow the same patterns of those for the flat-plate case. In addition, at section $X = 40$, the vibrational temperature for the $h = 9$ mm case has almost reached the equilibrium at the vicinity of the lower surface. In what follows, at section $X = 48$, the vibrational

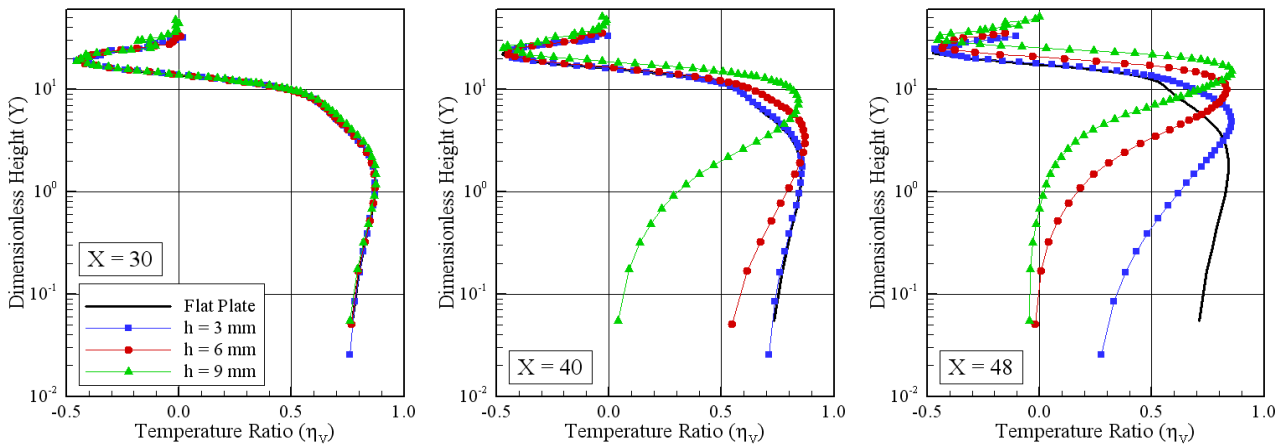


Figure 5. Distribution of η_V profiles for three sections along the step lower surface as a function of the height h .

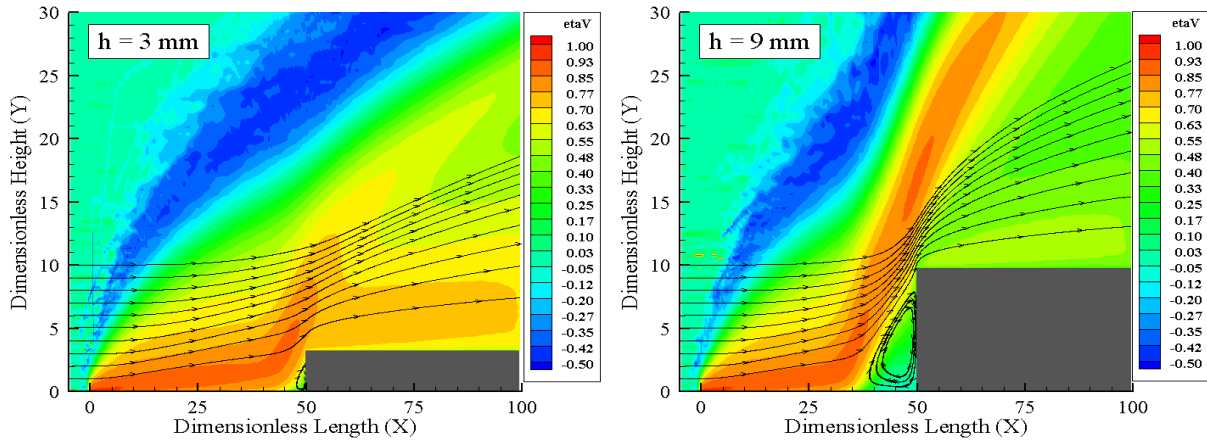


Figure 6. Non-equilibrium between vibrational and translational temperatures, η_V , for a hypersonic flow over forward-facing steps with height h of 3 mm (left) and 9 mm (right).

temperature for the $h = 6$ mm case comes to the thermal equilibrium, since $\eta_V \approx 0$. Nevertheless, for the $h = 3$ mm case, the vibrational temperature has not reached equilibrium yet. This occurs because the collision frequency rate is below the rate required for maintenance of the continual drop in temperature in order to achieve the equilibrium. Of particular interest is the η_V behavior in the outer part of the shock wave. In this region, $\eta_V < 0$, indicating that the vibrational temperature is slightly larger than the translational temperature.

In order to bring out the essential features of the thermal non-equilibrium associated with vibrational temperature, Fig. 6 displays the contour map for η_V at the vicinity of the forward-facing steps defined by height h of 3 and 9 mm. Similarly to the previous case, the distribution for h of 6 mm will not be presented.

Distributions for η_X and η_Y are depicted in Figs. 7 and 8 for the same three sections along the lower surface of the steps. It may be inferred from these figures that the profiles are qualitatively similar to those in Figs. 3 and 5 in the sense that the presence of the steps affects the temperature behavior upstream the frontal faces. Also, another flow peculiarity is related to the absolute values observed for η_X and η_Y . The temperature T_X , based on the velocity component in the x -direction, is larger than the temperature T_Y , based on the velocity component in the y -direction. The reason for that is because the velocity difference between the two groups of molecules in the shock wave, related to the near bimodal distribution mentioned earlier, is basically along the x -axis.

In an effort to emphasize interesting features of the thermal non-equilibrium associated with kinetic temperatures based on the velocity component in the x - and y -directions, Figs. 9 and 10 demonstrate contour maps for η_X and η_Y , respectively, at the vicinity of the forward-facing steps defined by height h of 3 and 9 mm. Contour maps for the whole flowfield confirm thermal non-equilibrium in the boundary layer and inside the shock wave.

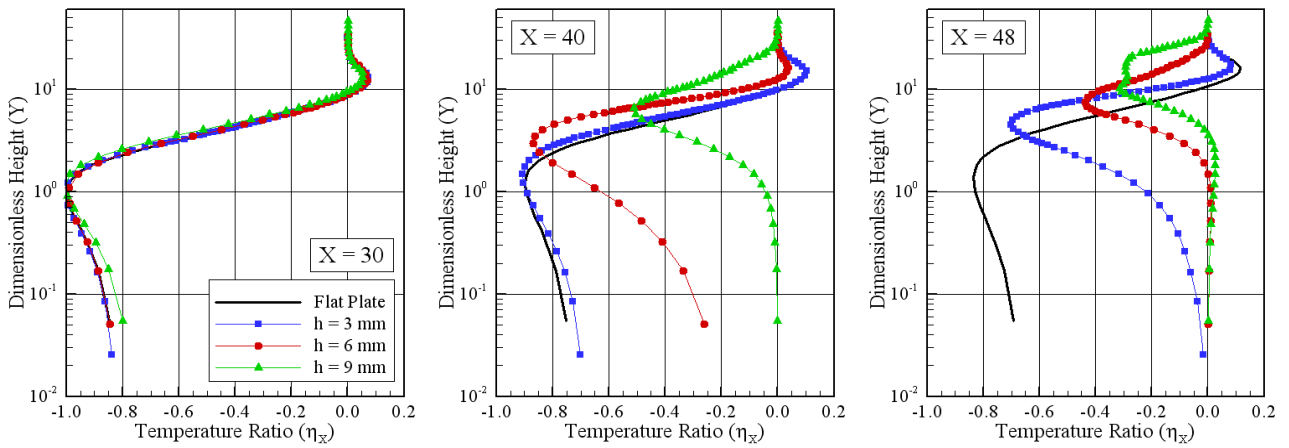


Figure 7. Distribution of η_X profiles for three sections along the step lower surface as a function of the height h .

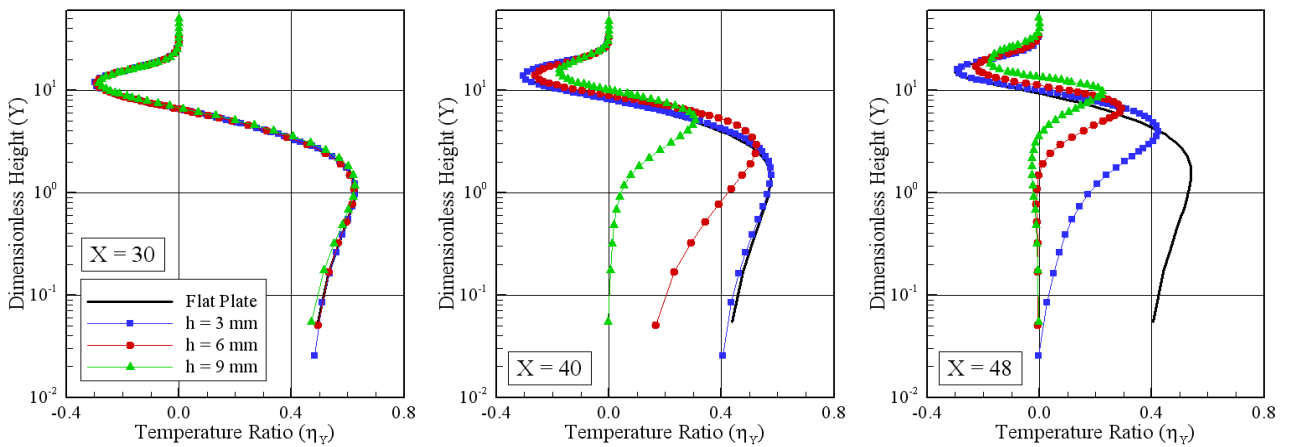


Figure 8. Distribution of η_Y profiles for three sections along the step lower surface as a function of the height h .

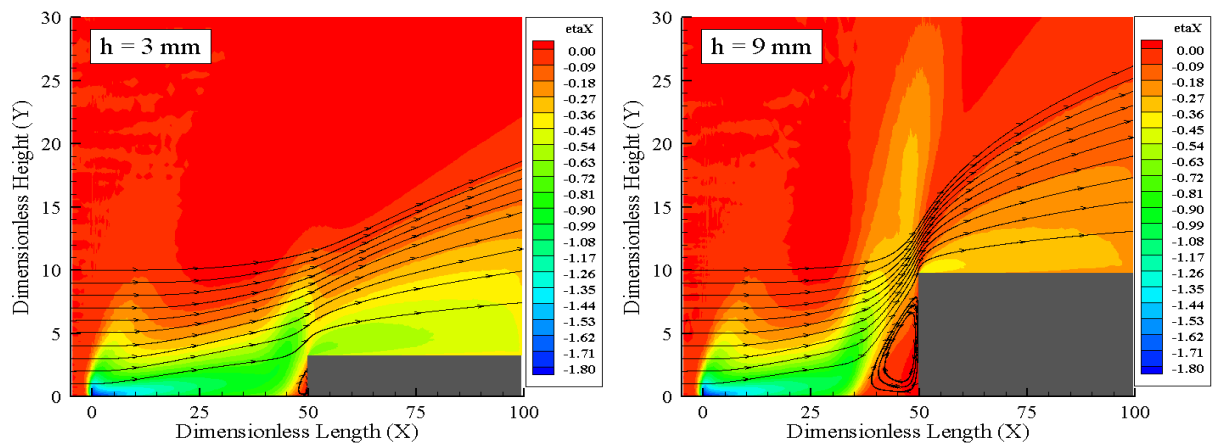


Figure 9. Non-equilibrium between “parallel” and translational temperatures, η_X , for a hypersonic flow over forward-facing steps with height h of 3 mm (left) and 9 mm (right).

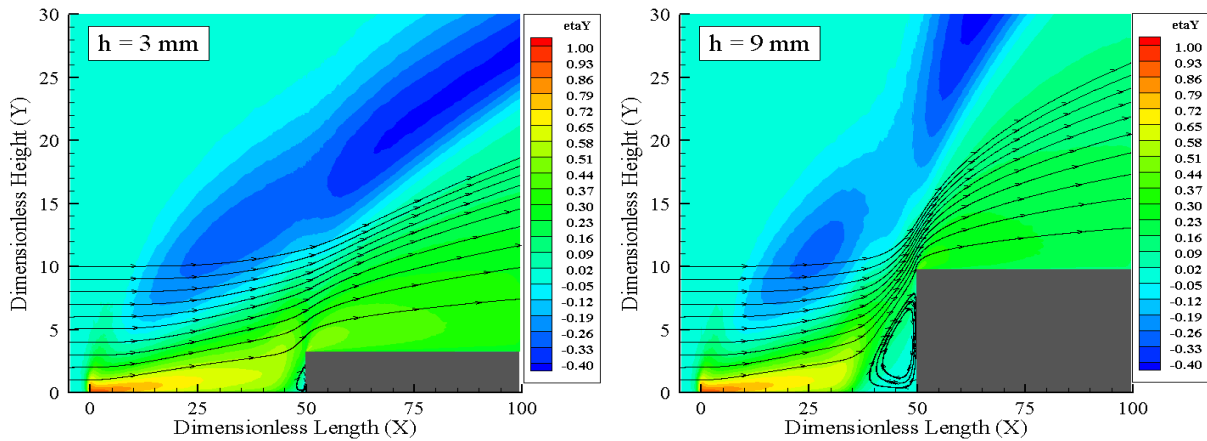


Figure 10. Non-equilibrium between “normal” and translational temperatures, η_Y , for a hypersonic flow over forward-facing steps with height h of 3 mm (left) and 9 mm (right).

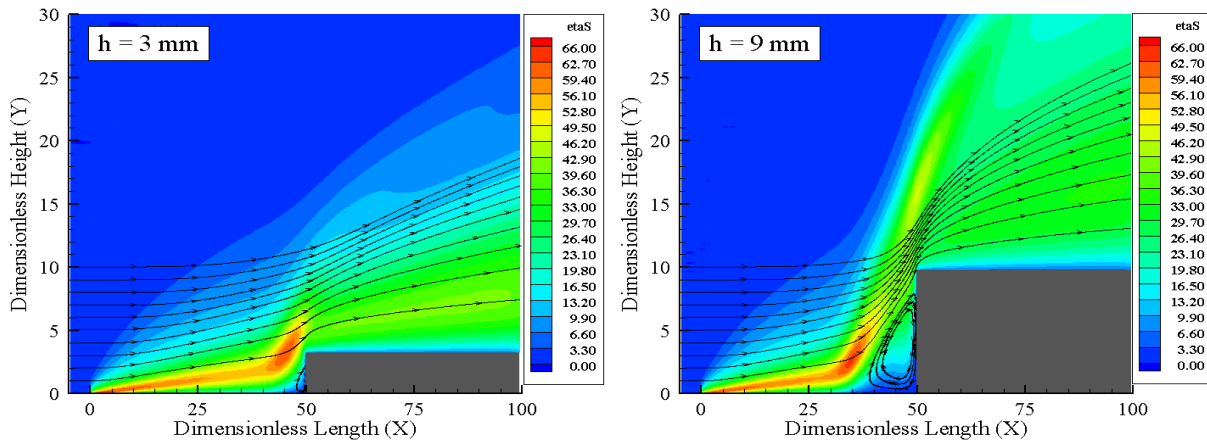


Figure 11. Contour map for entropy parameter, η_S , for a hypersonic flow over forward-facing steps with height h of 3 mm (left) and 9 mm (right).

Having a clear qualitative picture of the flow patterns associated with the thermal non-equilibrium between rotational, vibrational, “parallel”, “normal”, and translational temperatures, it proves convenient to assess the overall performance of entropy. In this fashion, an entropy parameter is defined as follows,

$$\eta_S = \frac{p/p_\infty}{(\rho/\rho_\infty)^\gamma} - 1 \quad (12)$$

where γ is the specific heat ratio.

Figure 11 illustrates the entropy contour in the flow along with some typical streamlines around the forward-facing steps defined by height h of 3 and 9 mm. According to these plots, the entropy generation is positive due to the flow compression through the shock wave. It is very encouraging to observe that at the vicinity of the step base, the entropy parameter η_S approaches zero, i.e., the flow is basically isentropic.

5. CONCLUDING REMARKS

In the current study, a rarefied hypersonic flow over forward-facing steps has been investigated by using the Direct Simulation Monte Carlo (DSMC) method. The simulations provided information concerning the nature of the thermal non-equilibrium effects in the flowfield around the steps. The impact of non-equilibrium between rotational temperature, vibrational temperature, “parallel” temperature, “normal” temperature, and translational temperature was investigated for

frontal-face height h from 3 to 9 mm, which corresponded to Knudsen numbers in the transitional flow regime.

According to the investigation, a thermal non-equilibrium flow was found inside the boundary layer and the shock wave. It was found that, at the vicinity of the step base, the flow is in thermal equilibrium. In this region, rotational temperature, vibrational temperature, “parallel” temperature, and “normal” temperature, basically reach the same value observed for the translational temperature. In addition, the results showed that entropy generation region is associated with the thermal non-equilibrium region in the flowfield.

6. ACKNOWLEDGEMENTS

The authors would like to thank the financial support provided by CNPq (Conselho Nacional de Desenvolvimento Científico e Tecnológico) under Grant No. 473267/2008-0.

7. REFERENCES

- Alexander, F. J., Garcia, A. L., and Alder, B. J., 1998. “Cell Size Dependence of Transport Coefficient in Stochastic Particle Algorithms”. *Physics of Fluids*, Vol. 10, No. 6, pp. 1540–1542.
- Alexander, F. J., Garcia, A. L., and Alder, B. J., 2000. Erratum: Cell Size Dependence of Transport Coefficient in Stochastic Particle Algorithms. *Physics of Fluids*, Vol. 12, No. 3, pp. 731-731.
- Bejan, A., 1988. “Advanced Engineering Thermodynamics”. John Wiley and Sons.
- Bird, G. A., 1981. “Monte Carlo Simulation in an Engineering Context”. *Progress in Astronautics and Aeronautics: Rarefied gas Dynamics*, ed., Fisher, S. S., Vol. 74, part I, AIAA New York, pp. 239–255.
- Bird, G. A., 1989. “Perception of Numerical Method in Rarefied Gasdynamics”. *Rarefied Gas Dynamics: Theoretical and Computational Techniques*, eds., Muntz, E. P., Weaver, D. P., and Capbell, D. H., Vol. 118, *Progress in Astronautics and Aeronautics*, AIAA, New York, pp. 374–395.
- Bird, G. A., 1994. *Molecular Gas Dynamics and the Direct Simulation of Gas Flows*, Oxford University Press.
- Borgnakke, C., and Larsen, P. S., 1975. “Statistical Collision Model for Monte Carlo Simulation of Polyatomic Gas Mixture”. *Journal of Computational Physics*, Vol. 18, No. 4, pp. 405–420.
- Garcia, A. L., and Wagner, W., 2000. “Time Step Truncation Error in Direct Simulation Monte Carlo”. *Physics of Fluids*, Vol. 12, No. 10, pp. 2621–2633.
- Grotowsky, M. G., and Ballmann, J., 2000. “Numerical Investigation of Hypersonic Step-Flows”. *Shock Waves*, Vol. 10, pp. 57–72.
- Hadjiconstantinou, N. G., 2000. “Analysis of Discretization in the Direct Simulation Monte Carlo”. *Physics of Fluids*, Vol. 12, No. 10, pp. 2634–2638.
- Leite, P. H. M., 2009. “Direct Simulation of the Step Influence on a Reentry Vehicle Surface (in Portuguese)”. MS Dissertation, INPE.
- Leite, P. H. M., and Santos, W. F. N., 2009a. “Direct Simulation of Low Density Hypersonic Flow over a Forward-Facing Step”. 20th International Congress of Mechanical Engineering, COBEM 2009, November 15–20, Gramado, RS, Brazil.
- Leite, P. H. M., and Santos, W. F. N., 2009b. “Numerical Investigation of Heat Transfer and Pressure Distribution of Hypersonic Flow over a Forward-Facing Step”. 30th Iberian-Latin-American Congress on Computational Methods in Engineering, CILAMCE 2009, November 5–8, Armação de Búzios, RJ, Brazil.
- Liepmann, H. W., Narasimha, R. and Chahine, M., 1964. “Theoretical and Experimental Aspects of the Shock Structure Problem”. *Proceedings of the 11th International Congress of Applied Mechanics*, edited by H. Gortler, Munich, Germany, pp. 973–979.
- Mates, R. E., and Weatherston, R. C., 1965. “Definition of Temperature in Nonequilibrium Process”. *Physics of Fluids*, Vol. 8, No. 4, pp. 657–662.
- Nestler, D. E., Saydah, A. R., and Auxer, W. L., 1969. “Heat Transfer to Steps and Cavities in Hypersonic Turbulent Flow”. *AIAA Journal*, Vol. 7, No. 7, pp. 1368–1370.
- Pullin, D. I., and Harvey, J. K., 1977. “Direct Simulation Calculations of the Rarefied Flow Past a Forward-Facing Step”. *AIAA Journal*, Vol. 15, No. 1, pp. 124–126.

8. Responsibility notice

The authors are the only responsible for the printed material included in this paper.